International Journal of Advanced Computer Science, Vol. 4, No. 1, Pp. 15-25, Jan., **2014**.

Very High Resolution NeuroElectric Brain Imaging Realized by Referee Consensus Processing

Don Krieger, Malcolm McNeil, Jinyin Zhang, Ava Puccio,
Walter Schneider, Xin Li, &David O. Okonkwo

Manuscript
Received:
31,Oct., 2013
Revised:
10,Dec.,2013
Accepted:
12,Dec.,2013
Published:
15,Jan.,2014

Keywords
MEG, nonlinear, optimization, functional brain mapping, grid computing, concussion, brain injury.

Abstract— Electrical current flow within populations of neurons is a fundamental constituent of brain function. The resulting fluctuating magnetic fields may be sampled noninvasively with an array of magnetic field detectors positioned outside a patient's head. This is magnetoencephalography (MEG). Each source may be characterized by 5-6 parameters, the xyz location and the xyz direction. The magnetic field measurements are nonlinear in the location parameters; hence the source location is identifiable only via search of the brain volume. When there is one or a very few sources, this may be practical; solutions for the general problem are weak.

Referee consensus is a new method which enables identification of one source at a time regardless of the number and location of others. This "independence" enables solution of the general problem and insures suitability to grid computing. The computation scales linearly with the number of nonlinear parameters.

MEG recordings were obtained from volunteers while they performed a cognitive task The recordings were processed on the Open Science Grid (≈150 CPU hours/sec of data). On average 500-1500 sources were active throughout. Statistical analyses demonstrated < 2 mm resolving power[1] and very strong findings ($p < 0.02^{400}$) when testing for task specific information in the extracted virtual recordings from each individual. 3D maps of differential activation, neuroelectric tomography, provide a very high resolution functional imaging modality which compares favorably with functional magnetic resonance imaging (fMRI).

Referee consensus is applicable widely to measurement systems including microwave telescope imaging, seismic tomography, and financial market linkage identification. Applicability requires: (1) The measurements are linear in at least one parameter of each "source." (2) Each source is detectable at multiple sensors. (3) A sequence of measurements in time is available.

1. Introduction

Electrical current flow within populations of neurons is a fundamental constituent of brain function. The resulting fluctuating magnetic fields may be sampled noninvasively with an array of magnetic field detectors positioned outside a patient's head. This is magnetoencephalography (MEG).

The signal at each MEG sensor is a weighted sum of the magnetic fields produced by sources within the brain, i.e. the relationship between the measurements and the amplitudes of the current sources is linear. But the number and locations of the sources are generally unknown and the relationship between the measurements and the source location coordinates is nonlinear [1]. These issues pose fundamental unsolved problems with handling and interpreting MEG signals.

In restricted special cases the data is manipulated so that plausibly the activity of only a single source is a significant contributor to the MEG. In these cases, the widely accepted Equivalent Current Dipole (ECD) localization is applicable. A single point source current dipole is assumed, requiring estimation of 5-6 parameters (3 location coordinates and 2-3 current amplitude components). The parameter estimation is typically accomplished using an iterative gradient search method for all 5-6 parameters. The accuracy of this method is vulnerable to either extraneous sources or noise in the data. This forces the analyst to average the data synchronized to an event and thereby reduce the quantity of information which may be extracted by a factor of 100 or more.

For the general multiple source problem, many investigators have opted to use methods with which thousands of point sources are estimated in a single operation, e.g. MNE [2], LORETA [3-4], VESTAL [5-6]. This approach provides a solution to the localization problem by including source locations with sufficient density to insure that no source is more than a few mm from one of them. But these methods produce thousands of parameters from hundreds of data points; they are under fit, i.e. poorly posed. Because of this both localization accuracy and the ability to resolve sources which are near each other is weak. Furthermore these methods are also vulnerable to noise in the data, again forcing up front averaging with consequent loss of information.

[1] Linear dimensions are represented in this standard form. Volume dimensions are represented throughout in terms of the length of a side, e.g. $8mm^3$ instead of ½ cc, ½ cm^3 or 512 mm^3.

This work was supported by the Pittsburgh Foundation, the Aberdeen Army Research Laboratory, the Extreme Science and Engineering Discovery Environment (XSEDE), which is supported by National Science Foundation grant number OCI-1053575, and the Open Science Grid, which is supported by the National Science Foundation and the U.S. Department of Energy's Office of Science.

Don Krieger, Malcolm McNeil, Ava Puccio, Walter Schneider, and David O. Okonkwo are with the University of Pittsburgh. Jinyin Zhang was with Carnegie Mellon University and is now with Google. Xin Li is with Carnegie Mellon University. (kriegerd@upmc.edu)

Referee consensus is used in a manner which is comparable to single source localization. But it has much less vulnerability to the presence of either extraneous sources or noise. And it is dimensionally well-posed. These properties enable (1) application to single trial data and (2) resolution of sources < 2 mm apart.

A formal treatment of the method is presented followed by results of its application to the MEG problem. The discussion details why the method works, the generalized version of the method for handling lagged relationships, and applications to other problems.

2. Methods

A. Experimental Methodology. Under University of Pittsburgh IRB approval (PRO09040294), 26 participants included 16 with history of concussion were enrolled in this study. Written informed consent was obtained after which all volunteers sat for MEG recordings while performing the task. Either MRI (23) or CT (3) was used for anatomic localization.

MEG recordings were acquired in the UPMC Brain Mapping Center with a 306-channel sensor array (Neuromag VectorView, Elekta Inc., Stockholm, Sweden) in a magnetically shielded room (Imedco, Hagendorf, Switzerland). Data sampling rate was 1000 Hz with front end high and low pass filter settings: 0.1-330 Hz. Line noise was removed from the raw MEG at 60, 120, 180, 240, 300 Hz using multiple regression [7].

With continuous MEG recording, each volunteer performed a visual choice task (Figure 1) controlled by EPrime 2.0 (Psychology Software Tools; Pittsburgh, PA). Each trial consisted of one of 8 sentences followed by 3 consecutive test figures to which a rapid response was given. Each sentence consisted of 5 words: "The blue/green circle/square is above/below."

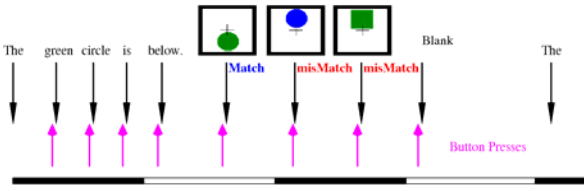

Fig. 1. A sample trial is shown. The bar at the bottom is 4 sec long. The black arrows indicate stimuli. The magenta arrows indicate responses to the preceding stimulus. The 2nd-5th word stimuli were triggered by a button press with the index finger. If the test figure matched the sentence, the response was a button press with the index finger. If not, the response was a button press with the middle finger.

All presentations were placed on a white background. 8 blocks of 40 trials were presented. It was assumed that within each block of 40 trials (~4 min) the head was fixed. The task with all recorded events is schematized in Figure 1. The transition from each stimulus to the next was self-paced, i.e. triggered by a button press (Brain Logics Fiber Optic Button Response System, Psychology Software Tools, Pittsburgh, PA). With each button press, the preceding stimulus, word or test figure, disappeared for 2 screen refresh cycles (~33 msec) before presentation of the next stimulus. Following the button press indicating the match/mismatch choice for the 3rd test figure, the screen was blank (white) for 1.0 sec with the fixation point appearing halfway through this interval.

B. Referee Consensus Optimization. The referee consensus cost function is a measure of local curvature in the space of a nonlinear search. The search space is a vector field over the volume of the brain. The vectors in this work are 80 point functions, the 80 msec time courses of neuroelectric currents.

The dimensionality of the domain of the space is 3, the x, y, and z coordinates of a single current dipole, A. Each 3D point for which the local curvature is positive is identified as a source [G]. The locality of the referee consensus cost function [4.A] enables identification of a single source at a time in the presence of numerous unknown simultaneously active sources. This independence ideally suits the referee consensus search to computational grid implementation.

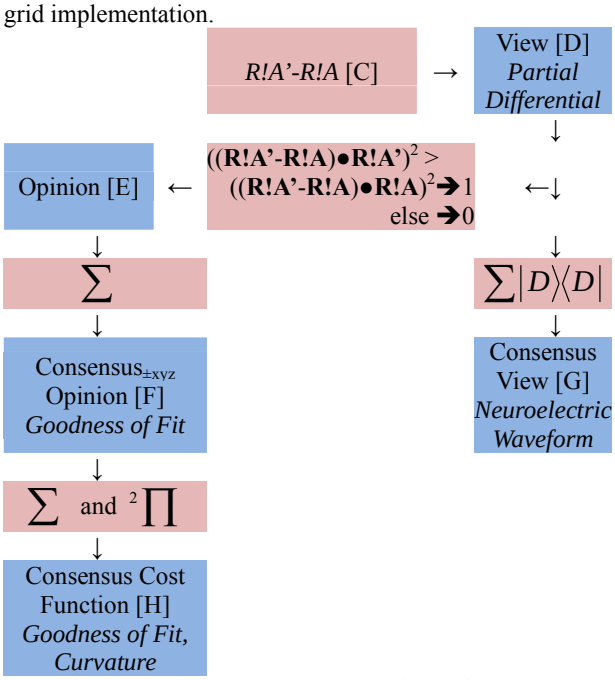

Fig. 2. The sequence for testing one 3D point of the search space, **A**, for the presence of a neuroelectric source. Referee consensus steps (blue) and numeric operations (mauve) are shown. References are shown to sections detailing each entry.

The search proceeds one 3D location, **A,** at a time. The cost function, referee consensus, is constructed from multiple measures of deviation from an absolute standard, zero. Each of these referee views [D] is the output of the difference filter for a referee, *R!A'-R!A,* where the filter is applied to an 80 msec MEG recording to produce the 80 msec time course of a current dipole, **R!A'-R!A**[3]. This difference filtering operation produces a partial differential. Since *R!A* has a zero [1.A] at the search space test location, **A,** the numerator of the partial differential is an estimate of the amplitude of the current source. The denominator is the

[2] This represents the products of the 6 p-values to achieve $p < 10^{-12}$.

[3] A filter is represented in italics, e.g. *R!A.* The 80 msec time course of a current dipole resulting from the application of *R!A* to an 80 msec MEG data segment is represented in bold, e.g. **R!A**.

1 mm line segment, **A'-A**[4]. In this work, there are 3 nonlinear variables, the xyz coordinates of **A**. 6 views (partial differentials) are computed for each referee using 6 different **A'**s, displaced from **A** ±1 mm along the x, y, and z axes: $_{+x}$**A', **$_{-x}$**A', **$_{+y}$**A', **$_{-y}$**A', **$_{+z}$**A', **$_{-z}$**A'.**

The referee view is transformed to an opinion by a 1 bit digitization operation [E]. The opinions for each of the 6 differentials are summed separately to produce 6 consensus$_{\pm xyz}$ opinions [F]. Each of these is a measure of "goodness of fit" since each quantifies how well the referee views are distinguishable due to a neuroelectric current at **A**. The presence of a source at **A** is accepted only if all 6 consensus opinions are significantly greater than ½ the number of opinions[5], i.e. the curvature is positive. If one or more of the consensus opinions is significantly less than ½, then **A** is a saddle point and there is a presumed source nearby. The direction to move for the next **A**, the "gradient" for the search, is determined by the significant consensus opinions of both types.

C. Formalism for a Referee Consensus System. A referee consensus system is a multiple sensor measurement system in which each sensor functions in a linear range. This enables representing the system as a set of linear equations, one for each sensor. The additive terms in the equations are functions of each of the sources; the number of these terms is generally unknown. Each function has one or more nonlinear parameter and at least 1 linear parameter[6]. "Best" values for the "location," the nonlinear parameters[7], are identified by trial and error, i.e. a search. At each step of the search the values of the nonlinear parameters are fixed, enabling solution for the remaining linear parameters using the linear formulation detailed below.

A referee consensus system is formulated as a set of linear regression equations: $\vec{B}^{\mathsf{T}} = \mathbf{H}\vec{D}^{\mathsf{T}} + \vec{E}^{\mathsf{T}}$. The elements of $\vec{B}$ are the measurements (known). The elements of $\vec{D}$ are the linear source variables (to be estimated via ordinary least squares regression). The elements of $\vec{E}$ are the errors in the estimates. Each element of $\mathbf{H}$, the h_{jk}, are nonlinear functions of the parameters that characterize the j^{th} sensor and the k^{th} source. The equations are solvable only when these nonlinear parameters are fixed so that the h_{jk} are numbers. For the referee consensus method, the existence and the values of the parameters of one source at a time are determined. All other sources included in the system estimate are either at fixed dummy "referee" locations or at known source locations which are included to reduce the errors[8].

The formulation of a referee consensus system must include at least 2 sources: (1) the target (k^{th}) source, the one for which the nonlinear parameters are to be found by search and (2) at least one referee location. Each referee must be "correlated" to the target location, i.e. the dot products of the columns of $\mathbf{H}$ corresponding to the referees with the columns for the target location must be non-zero [1.B].

The ordinary least squares solution for $\vec{B}^{\mathsf{T}} = \mathbf{H}\vec{D}^{\mathsf{T}} + \vec{E}^{\mathsf{T}}$ is $\vec{D}^{\mathsf{T}} = \left(\left(\mathbf{H}^{\mathsf{T}}\mathbf{H}\right)^{-1}\mathbf{H}^{\mathsf{T}}\right)\vec{B}^{\mathsf{T}}$, i.e. the k^{th} element of $\vec{D}$ is a weighted sum of the measurements, $\vec{B}^{\mathsf{T}}$, where the weights are the entries in the k^{th} row of $\left(\mathbf{H}^{\mathsf{T}}\mathbf{H}\right)^{-1}\mathbf{H}^{\mathsf{T}}$. Each of these rows is then a linear filter. Effectiveness of the referee consensus method relies critically on the fact that the k^{th} filter has zero gain for contributions to the measurements from all of the entries in $\vec{D}$ except d_k. Section 1.A contains a proof.

D. Referee View. An estimate of the time course for a putative source at **A** from the viewpoint of referee **R** is computed as follows. (1) The system is solved for sources at the target location, **A**, and a referee, **R**. The filter[9] for **R**, *R!A*, is applied to an 80 msec MEG time segment in this work to produce the time series, **R!A**. There is no contribution to this sequence from a source at **A** since *R!A* has zero gain for a source there [1.A]. Hence we refer to this filter as: "R not A." (2) The system is solved for the same referee, **R**, but a different target location 1 mm from **A**, **A'**. Again the filter for **R** is applied to the sequence of measurements but this time there is a contribution from **A** since it was not included in the model. This time series is **R!A'**.

R!A'-R!A is an estimate of the time course of a source at **A,** $d_k[t], t = 1,\ldots,80$. Viewed as the output of the difference filter, *R!A'-R!A*, **R!A'-R!A** is a partial differential whose numerator is proportional to $d_k[t], t = 1,\ldots,80$ and whose denominator is the 1 mm line segment, **A'-A**. There

---

[4] The domain of the search was artificially constrained to a 1 mm cubic grid.

[5] In this work 90 referee locations are used. For each of these there are 2 referees oriented at right angles to each other which are constrained to be correlated in this work; hence the statistics are conservatively handled using ½ counts, 90 rather than 180. 57 of 90 ($p \approx 0.007$) was used as the threshold for significance. This results in a threshold for significance for positive curvature, i.e. for accepting the presence of a source, of $0.007^6 < 10^{-12}$.

[6] For the magnetic field due to a current dipole in a uniformly conducting sphere [1] each source is characterized by 5 parameters. 3 of these are nonlinear, i.e. the xyz coordinates of the location of the source. The 2 linear parameters are the 2 components of the amplitude of the current in the tangent plane. This physical model precludes detection of the radial component of an intracranial current source.

[7] One or more linear parameter may be identified by search along with the nonlinear ones. This could be required if there are too few sensors to enable inclusion of the all the linear parameters as linear source variables in the regression formulation.

[8] This error reduction approach is not used in this work.

[9] For the MEG problem, it is natural to handle these variables 2 at a time, i.e. the two orthogonal components of a current dipole. For simplicity but without loss of generality, we describe formation of the referee template for a single variable at a time.

are 6 of these views for each referee, one for each of the 6 line segments where **A'** = **A** ±1 mm along the x, y, and z axes.

E. Referee Opinion. If there is in fact a source at **A**, it should contribute to **R!A'** but not to **R!A**. The referee opinion as to the presence of a source at **A** is computed by the following 1-bit transform: If $((\mathbf{R!A'}-\mathbf{R!A})\bullet\mathbf{R!A'})^2 > ((\mathbf{R!A'}-\mathbf{R!A})\bullet\mathbf{R!A})^2$, the opinion = 1, i.e. there is a source present at **A** from the view of this referee. Otherwise the opinion is 0. There are 6 opinions, one for each of 6 views.

F. Referee Consensus$_{\pm xyz}$ Opinion. There are 6 referee consensus opinions, one for each of the 6 **A'**s. Each is computed by counting the referee opinions for the corresponding **A'**. The probability of getting a particular count is interpretable as one would interpret the flip of a fair coin. The expected value for K flips is K/2, e.g. the chance of getting 57 or more heads (1's) out of 90 referee opinions ≈ 0.007. This is the threshold p-value used in this work for each of the 6 consensus opinions for acceptance of the existence of a source at **A**, i.e. each of the 6 measures of goodness of fit is significant.

G. Referee Consensus View: The Template. The individual referee views are combined into a consensus view. Averaging was not used because the sign of each view was unconstrained. Rather the outer products of the views with themselves were used to generate a sum of squares and cross products matrix: $\sum_{m=1,1080} |D_m\rangle\langle D_m|$. The first eigenvector of this matrix was used as the consensus view.

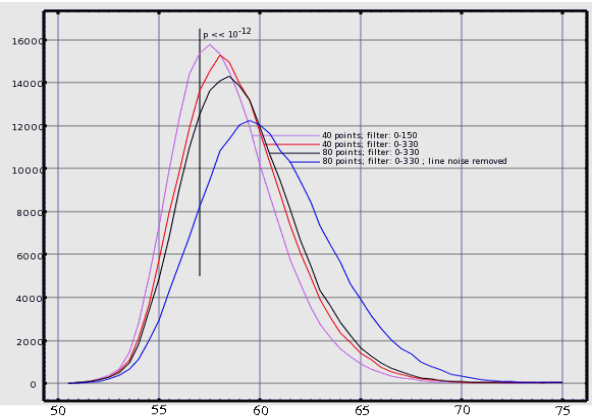

Fig. 3. The distribution of values of the average referee consensus metric, $0 \le \sum(consensus\_opinion_{\pm xyz}/6) \le 90$, is ≈ symmetric and improves with both template length (40:red → 80:black), reduced low pass filtering (150 Hz: mauve → 330 Hz: red), and with removal of line noise from the MEG (blue). The vertical bar at 57 out of 90 for each of 6 tests has a nominal $p < 10^{-12}$ (see text). A shift to the right, i.e. increase in referee consensus, reflects improved goodness of fit.

H. Referee Consensus Cost Function. **A** was accepted as the location of a source only if the threshold p-value of 0.007 was reached for all 6 **A'**s, i.e. the curvature of the vector space at **A** is positive. Hence the probability of accepting a source by chance was $p < 0.007^6 < 10^{-12}$. If one or more consensus$_{\pm xyz}$ opinion was significantly less than ½, less than 33 out of 90, **A** is a saddle point suggesting that there is a nearby source not at **A.** The gradient for the continued search was computed using the significant consensus$_{\pm xyz}$ opinions of both types.

I. Parameter constraints. A limited exploration enabled selection of key parameters of the calculation which are only partially constrained otherwise. Figure 3 shows typical distributions of values that were obtained for the referee consensus depending on parameter selection. These parameters are listed with the constraints selected from the results summarized in the figure 3: (1) length of a data segment (80 msec), (2) band pass filtering applied to the MEG (none), and (3) removal of line noise from the MEG (yes). The substantive shifts to the right in the figure represent improved goodness of fit, i.e. greater referee consensus.

J. Referee Consensus Data Processing. For each trial, 6 560 msec data segments were selected for extraction of virtual recordings using referee consensus processing. The search for active MEG sources was conducted for 80 msec time segments, one at a time, each overlapping the previous segment by 40 msec. The brain volume absent a sphere with 15 mm radius at the center of the head[10] was divided into ≈ 3000 ½ cm^3 cubes. Each instance of the search routine, mvrXS, searched the data from 40 target figures for one of these ½ cm^3 volumes.

Each such job required about 1 hr of computing time. Processing the data for each volunteer required: 3000 voxels (8mm^3 ≈ ½ cm^3) x 8 (trials blocks) x 3 (target figures) ≈ 72,000 jobs. The data flow and control software are shown in Figure 4.

Files on the Master and on the front-end are used both as flags and as tokens by the scripts running at both ends. Both the names and contents of these files are used to communicate control information. That information is accessed by polling using standards file operations, e.g. mv, filetest, cat, ls. mv is used to adjudicate race conditions when there are multiple instances of scripts using a token.

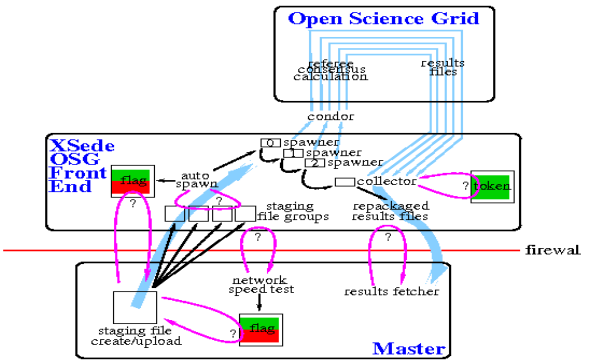

Fig. 4. OSG data flow (light blue arrows) and job control. Magenta arrows represent polling loops; question marks indicate the objects which are polled. Black arrows represent script functionality, e.g. file operation and process spawning.

The scripts spend most of their time idled via the system function, sleep. The Linux sleep may be passed an

[10] Due to geometric and other physical constraints, magnetic fields produced near the center of the head are undetectable. Efforts to measure them result in numeric instability in the computational algorithms.

arbitrary precision floating point number which may be used to encode current script status information. That information may then be accessed by a monitor script which polls the system process list with ps.

The calculations were hosted by the Open Science Grid (OSG). Typical ongoing grid usage for this work over 100 days is shown in Figure 5: ≈5.4 million hours of clock time. This amounts to ≈4% of the total grid usage for that period.

mvrXS was written in Fortran 77 and compiled with gfortran. The dot product routines were optimized. The eigenvector decompositions and matrix inversions using Cholesky factorization were handled at 64 bit precision using LaPack [8].

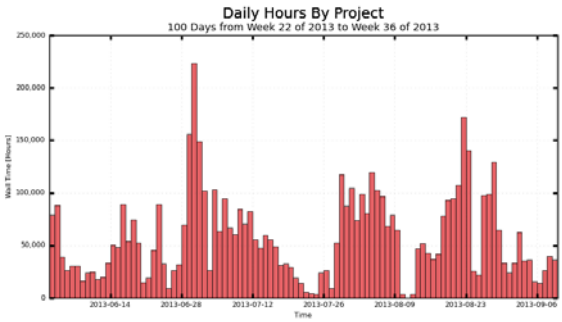

Fig. 5. 100 days of typical ongoing OSG usage for this project is shown. The total is ≈5.4 million cpu hours, amounting to ≈4% of the total OSG usage.

All job control, results aggregation and transport, and housekeeping functions were handled by tcsh scripts. These were developed incrementally over several months with the following objectives:

1. Maintain sufficient pending jobs in the queue to utilize all available idle cycles (Figure 6).
2. Eliminate loss-of-results errors.
3. Minimize (a) network traffic, (b) front end scratch disk usage, (c) front end scratch disk access operations.
4. Minimize human oversight. This has been reduced from several per day to once per several days.
5. Tolerate faults: (a) network slowdowns, (b) front end scratch disk slowdowns, (c) front end reboot.

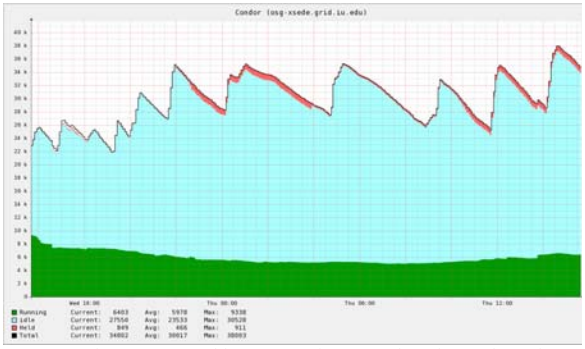

Fig. 6. Jobs are spawned in groups of ≈3000 when the total number in the queue falls below a set point, 8500. This gives rise to the typical thermostat-like saw tooth appearance of this 24 hour grid status graph.

Each instance of the executable required ≈ 300 Mbytes of core memory at run time. In addition each instance required network transport of ≈10 Mbytes of file data including the mvrXS static image, the MEG data segments, data specific tables, and results files. For each group of 3000 jobs, the MEG data segments were the same and accounted for ≈2/3 of the data transport demand. Since our jobs typically ran on only 5-20 facilities at a time, we were able to reduce this by ≈40% using the "SQUID" http transportation layer provided by many OSG resources which includes local file caching.

The calculation of the referee consensus requires the 4 steps listed below. In order to measure the gradient of the referee consensus, these were carried out 6 times, once for each point adjacent to the target location 1 mm along the x, y, and z axes. Note that for the MEG problem, there are 2 linear variables for each source location.

1. Compute 180 referee templates, 2 for each of 90 referee locations.
2. Compute the first eigenvector of the 180 templates. This is the referee consensus template.
3. Compute 180 referee metrics, 2 for each of the 90 referee locations.
4. Sum the referee metrics to obtain the referee consensus.

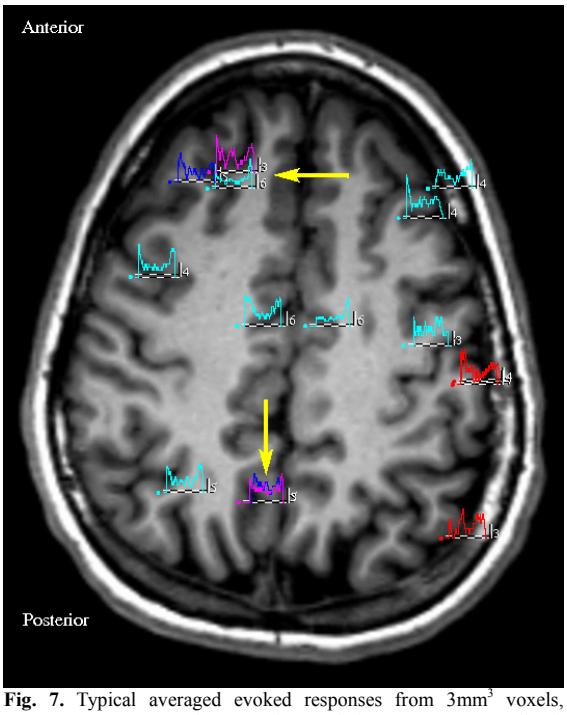

Fig. 7. Typical averaged evoked responses from 3mm^3 voxels, 300-500 80 msec waveforms. Time scale is 500 msec. Amplitude scale is indicated in amp^{-9}meters. Blue: Test figure and sentence were a match. Red: Test figure and sentence did not match. Aqua: Test figure was above the fixation point. Magenta: Test figure was below the fixation point. Vertical arrow: Vertical arrow: Coincident waveforms demonstrate processing delay. Horizontal arrow: Nearby (6 mm) waveforms show low correlation, i.e. high resolving power.

If there is, in fact, an MEG source present at a location, the two members of the corresponding pair are likely correlated with each other. We can estimate the chance of getting 114 or more out of 180 in the worst case, i.e. when they are perfectly correlated, by reducing the referee consensus by ½: I.e. the chance of getting 57 or more heads out of 90 flips of a fair coin is 0.007; the chance of

doing so 6 times in a row is $0.007^6 \approx 10^{-12}$. In addition the fairness of the "coin flips" is potentially compromised by correlations of the referees' transfer functions. Analysis of this potential bias is beyond the scope of this paper.

To identify the starting point for the search of each ½ cm^3 volume, referee consensus was applied once to 34 points scattered evenly through the cubic volume. A maximum of 6 steps guided by the gradient calculation was then allowed before terminating the search. Other efficiencies included applying laboriously generated tables piecemeal across time segments rather than storing their results or repeating them. Together these reduced the computational load by a factor of 40 compared to an exhaustive grid search.

3. Results

A. *Virtual recordings.* For each 80 msec time segment for each single trial, 500-1500 active sources were found. For each identified source, the xyz coordinates, the value of the referee consensus, the 80 point time series referee template, and the two components of the amplitude were stored for further analysis. Each of these 80 msec waveforms is viewable as a fragment of a single trial evoked response by the tissue at that location. Typical averages are shown in Figure 7.

The resolving power demonstrated in the figure was quantified as follows. The correlation was computed between all pairs of source that occurred simultaneously. The correlation was then plotted as a function of the distance between the members of the pair. Typical results from 3 subjects are shown in Figure 8. The figure demonstrates that the method resolves sources < 2 mm apart.

B. *Task specific information.* The presence of task specific information must be demonstrated in the single trial virtual recordings to validate the method. This was done separately for the virtual recordings from each volunteer.

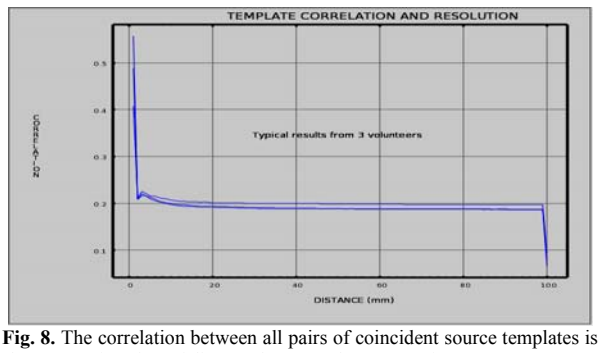

Fig. 8. The correlation between all pairs of coincident source templates is shown as a function of distance between the sources from 1 mm to 10 cm. The absolute value of the correlation was used in each case. The variance in the measure across all pairs was ≈ 0.02. These results demonstrate resolving power of < 2 mm. The results shown (3 subjects) were typical. The search was confined to a 1 mm grid covering the brain so 1 mm is the limit of the detectable resolving power.

The search volume was divided into cubic voxels. The number of identified sources in each voxel was counted (1) for test figure presentations which matched the sentence and (2) for test figures which did not match. The two counts within each voxel were then tested for equality using the χ^2 statistic. The ratio of the two counts over the entire volume was used as the expectation ratio[11]. These counts were made for a sequence of voxels sizes: $2mm^3$, 3, 4, 6, 8, 12, and 24.

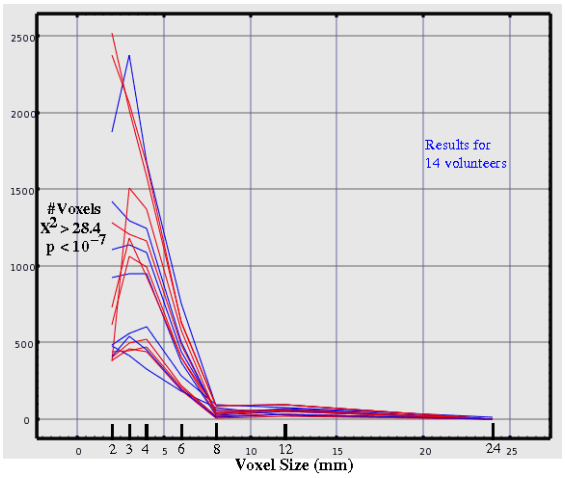

Fig. 9. Task specific information is preserved in single trial virtual recordings. The number of neuroelectric sources was counted within each voxel (1) for test figures matching the sentence and (2) for test figures which did not match. The number of voxels for which the counts were "different" is plotted on the y-axis ($\chi^2 > 28.4$, $p < 10^{-7}$). The voxel size is plotted on the x-axis.

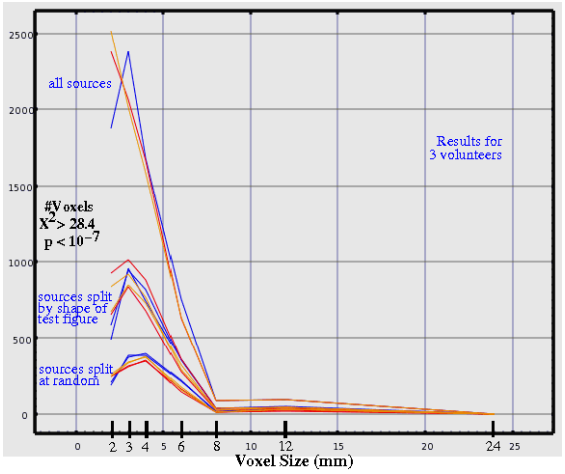

Fig. 10. Task specific information is preserved in single trial virtual recordings: overlap replication. The number of neuroelectric sources was counted within each voxel and tested for differences as in Figure 8. Results for the 3 individuals with the strongest findings are shown in red, blue, and orange. Results using all sources are most significant. The counts were repeated after splitting the sources at random. The pairs of traces are indistinguishable for each individual. The counts were repeated again after splitting the sources according to the shape of the test figure, square or circle. The traces for the each individual are now different and the results are more significant than when the division is at random.

The threshold for significance was set at $\chi^2 \geq 28.4$, $p \leq 10^{-7}$, to enable statistical inferences from the results from a

[11] This is more conservative than the use of the true expected ratio, i.e. the number of match/mismatch test figures.

single voxel. In the worst case considered, i.e. for $2mm^3$ voxels, ≈200,000 are required to cover the brain. In that case the chance that a single voxel out of 200,000 will reach the selected significance threshold is 0.02. Note in Figure 9 that the minimum number of voxels reaching the threshold is ≈400. The chance for that worst case is $p < 0.02^{400}$, i.e. astronomical. It can therefore be inferred with very high confidence that task specific information is preserved in the single trial virtual recordings from each volunteer.

A test was then run of the validity of the statistical method and its result. The identified neuroelectric sources were divided at random into 2 equal groups and the counts and calculations were repeatedly separately on each of the groups (Figure 10). For each subject the traces in each pair (1) show high significance[12] and (2) are indistinguishable from each other[13], validating the method and result.

A second test was run in which the identified neuroelectric sources were divided according to the shape of the test figure[14], circle or square (Figure 10). For each subject the traces in each pair (1) show more significance than for the random division and (2) they are readily distinguishable from each other. The finding of significance strongly supports the conclusion that task specific information is present in the virtual recordings. The facts that the significance is increased and that the traces are different for circle vs square test figures implies these voxels are "associative," i.e. they are differentially activated by the combination of match vs mismatch and circle vs square.

It is noteworthy that these findings provide strong evidence that (1) the resolving power[15] found here is $\leq 2mm^3$ and (2) the size of neuroelectric functional unit is $\leq 6mm^3$. This latter is inferred from the shape of the traces in Figures 9 and 10. Very few voxels $\geq 8mm^3$ reach significance whereas many $\leq 6mm^3$ do. See the discussion section for more on this.

C. *3D maps of differential activation.* Voxels for which the source counts demonstrate significance on the test for task specific information may be superimposed on a high quality structural MR scan, e.g. Figure 11. This produces a neuroelectric tomogram, NET, a 3D map of task specific differential activation. See the discussion section for comparison with functional MR Imaging, fMRI.

4. Discussion

The referee consensus method is computationally expensive. But that expenditure produces intracranial current measurements from single trial data that retain task specific information (Figs 9, 10, 11) and that distinguishes sources < 2 mm apart (Figure 8).

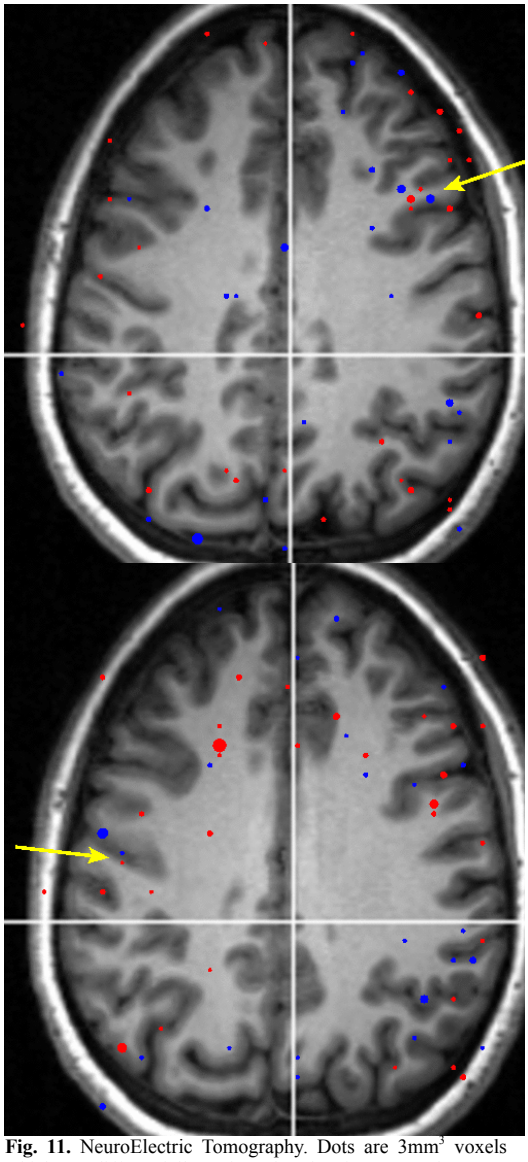

Fig. 11. NeuroElectric Tomography. Dots are $3mm^3$ voxels which are differentially activated as in Figs 9,10. Blue: Test figure matches the sentence. Red: Test figure does not match the sentence. Dots are shown only when $\chi^2 \geq 28.4$, $p \leq 10^7$. Upper panel is an MR slice 3mm superior to that shown in lower panel. Arrows indicate adjacent voxels with opposite differential activation. Images have standard medical orientation: anterior/poster =up/down; left/right = right/left.

A. Why does referee consensus work? Each referee's binary opinion is derived from the output of the difference between 2 filters with zeroes in the neighborhood of the source test location. Each of the 2 filters also has zeroes at all of the other referee locations whose "opinions" will be polled. The fact that almost all the zeroes are the same in both filters constrains their transfer functions to be similar throughout the search space. The primary differences are in

[12] As expected due to reduced counts and resultant reduced statistical power, the number of voxels for which the counts reach the statistical threshold is reduced.

[13] Given the extraordinary statistical strength of the findings, it is expected that the results should be very similar.

[14] Comparable results were obtained when the sources were divided according to the color of the test figure, green or blue, the position of the test figure, above or below the fixation point, or the whether the previous test figure was a match or a mismatch.

[15] Resolving power means the distance scale over which neuroelectric sources with different activity may be identified as different. This is in contradistinction to localization accuracy.

the neighborhood of **A,** the source test location [9]. The differencing operation therefore strongly attenuates the contribution of all sources outside the neighborhood of the source test location; each difference filter behaves as a signal space separator. This enables identification of one source at a time in the presence of an unknown but large number of active sources.

This same point may be seen by noting that $\mathbf{H}$, the lead field matrix [2.C], differs with the inclusion of **A** vs **A'** only in the 2 columns for the target location. Since locations **A** and **A'** are close to each other, these columns differ only slightly. In the work here, 90 referee locations with 2 columns each were included in $\mathbf{H}$. Hence $\mathbf{H}$ and the resultant filters, the rows of $(\mathbf{H}^T\mathbf{H})^{-1}\mathbf{H}^T$, were only slightly perturbed with the major difference in gains being in the neighborhood of **A**. This isolates the estimation of the referee template from the influence of other sources since the gains elsewhere are nearly equal for *R!A* and *R!A'*. Hence the difference operation attenuates the contribution of other sources as well as the contributions of instrument noise.

It is to be expected that the signal space separation properties of a difference filter will be imperfect in the sense that a source at a correlated location could produce a false identification. Correlation in the context of other MEG methods [2-6, 10-12] means that the magnetic fields from sources at the two locations are spatially correlated, i.e. they have a similar shape. But for a referee opinion, the magnetic field shape must be preserved over 80 msec. It is a measure of spatiotemporal goodness of fit. To defeat referee consensus, the interference must come from a spatiotemporally correlated source. This is likely far rarer than spatial correlation alone except in the neighborhood of **A**. There the spatial correlations are high and the temporal correlations may be also since neural populations near each other may display similar activity. This latter expectation is moderated by the surprisingly weak correlations found between nearby sources as shown in Figure 8. Furthermore the transfer functions of the difference filters used in the method [9] are particularly well suited to distinguishing nearby sources with high spatiotemporal correlation.

Figure 3 in the Methods section demonstrates marked increase in referee consensus, i.e. goodness of fit, when low pass filtering is relaxed from 150 Hz to 330 Hz. Improved performance with greater high frequency content (1) highlights the importance of the spatiotemporal fit, (2) implies that there is detectable neuroelectric content in the frequencies above 150 Hz, and (3) highlights the difference between referee consensus and other methods for which this effect is opposite.

Referee consensus is the sum of 1 bit quantities. This digitization provides robustness to the method, minimizing the effects of outliers.

The use of a sum over a large number of referees, i.e. 180 difference filters for each of 6 partial differentials, also minimizes the impact of biased "viewpoints." Such bias is potentially present for groups of referees which may produce correlated "opinions" due to their inter-referee spatial correlations. And if present this could degrade the statistical power of the method[16].

Each referee view requires application of a unique difference filter to the 80 msec MEG fragment. This produces an estimate of the activity of the neuroelectric current. There are 180 x 6 = 1080 of these estimates which are combined in a manner analogous to averaging with comparable signal/noise enhancement properties to produce the consensus view [2.G], a joint estimate of the neuroelectric waveform[17].

B. Referee consensus summary. Virtually all nonlinear optimization methods use a measurement error metric as the cost function. The standard to which the solution is fit is therefore imperfect since it is the measurements. And the minimum which is sought for the cost function is a global one. Referee consensus uses a perfect standard, zero.

Referee consensus defines a cost function, a measure of local curvature, over a search space whose domain's dimensionality is reduced to that required for a single source. This locality is a critical property since the number and location of sources which contribute to the measurements is, in general, unknown.

Referee consensus utilizes linear filters as do all "source space" methods in current use for the MEG problem. And it uses a search as does equivalent current dipole source localization [1]. But in other ways it is quite different: (1) Rather than using a single filter with unit gain for a target location, 1000+ differenced pairs of filters [2.D] are used for dummy (referee) locations, each with zero gain [2.C,1.A] at or very near the target location. (2) To decide if there is a source at a target location, a probabilistic measure of goodness of fit is constructed [2.E,2.F] from the output of 1000+ filter pairs for that target rather than using a measurement error metric [1] or a post-hoc test on the outputs of the filters for all of the targets [4,6,10]. (3) The time course of the activity at the target location results from a joint estimation procedure [2.G] applied to the output of all 1000+ filter pairs rather than from the output of a single filter.

C. Size dependence of differential activation, the neuroelectric functional unit. To validate the method it was necessary to demonstrate the presence of task specific information in the single trial virtual recordings. This was accomplished previously [9] using a two stage process to minimize the multiple comparison problem. The first stage [10] enabled identification of a restricted volume within which identified virtual recordings were used for further analysis. This was needed to narrow the statistical testing to virtual recordings from a brain region that was likely involved in the task. Otherwise an unrealizable global search would have been required. Multiple ANOVA was then applied to spectral estimators from the virtual recordings to test for significant task specific differences.

The simpler approach taken here was to count the

[16] Study of this problem is beyond the scope of the present work but will be undertaken and reported in the future.

[17] This operation is expected to produce signal/noise enhancement proportional to $1080^{½} \approx 30$.

number of identified sources in each voxel for different task conditions and then compare the counts. The large number of identified sources and the apparent high fidelity of the source estimates provided sufficient statistical power for a global search using voxels ranging from $24mm^3$ (≈100 voxels) to $2mm^3$ (≈200,000 voxels).

The results (Figures 9,10) parameterized on voxel size provide an estimate of the distance scale over which neurons cooperate to perform a task related function, i.e. the size of a neuroelectric functional unit. The number of voxels for which the counts show a significant difference shows a sharp increase at $6mm^3$ or smaller compared with $8mm^3$ or larger. This suggests $6mm^3$ as the upper limit for the size of a functional unit. The curves flatten out or turns down near $3mm^3$ but retains astronomical significance [18] for each individual at $2mm^3$.

D. Neuroelectric Tomography (NET) compared with functional MR Imaging (fMRI). Functional MR Imaging is the predominant functional brain imaging modality. The table shows the favorable technical comparison between fMRI and NET. But NET has yet to demonstrate its value in clinical usage. It is a new technology awaiting application as was fMRI 20 years ago. NET with its very high spatial and temporal resolving power is directly responsive to the findings of the 2013 NSF workshop on grand challenges in mapping the human brain [13].

	fMRI NeuroVascular	**NET NeuroElectric**	**fMRI/NET**
biological measure	tissue oxygenation	electric current	complement
measure type	scalar	vector	
3D spatial resolution	$\geq 5mm^3$	$< 2mm^3$	ratio: $> \mathbf{15}$
3D functional unit size	$\geq 5mm^3$	$\leq 6mm^3$	poor overlap
temporal resolution	≥ 50 msec	≤ 1 msec	ratio: $\geq \mathbf{50}$
further primary information	none	many traces for each voxel	
info extraction	resolution + more primary info		ratio: $> \mathbf{10^3}$
Voxel p-value ≈ statistical power	5×10^{-2}	10^{-7}	ratio: $> \mathbf{10^5}$

E. Other applications for referee consensus. Referee consensus is generally applicable to a wide class of measurement problems: (1) The core of these problems is that the number of sources whose activities are causing the measurements is unknown. (2) The measurements are linear in at least one parameter of each "source." (3) Each source is detectable in multiple sensors. (4) A sequence of measurements in time is available. In addition to the MEG problem referee consensus is applicable to microwave telescope imaging, ultrasound imaging, seismic tomography, active and passive SONAR imaging, neural network connectivity identification/analysis, and financial market linkage identification/analysis.

The formulation of referee consensus presented here is for the "instantaneous" method. The presumption is that the measurements at all sensors due to the activity of a single source are simultaneous. There are numerous systems for which this is not the case, i.e. when the action of a sources has different "times of flight" to different sensors. For instance seismic tomography is a problem that deals with time lags of minutes or more since a shock to the earth may be detected and localized using an array of accelerometers 1000's of miles apart [14].

The general referee consensus model which is used to handle lagged relationships between sources and measurements is the set of equations which describe the causal relationship between the sequence of actions in time of many discrete sources and the resultant sequence in time of the measurements. Each source is defined by 2 or more variables, 1 of which is called the amplitude[19]. The key departure from the instantaneous version is that the measurement and error vectors are sequences of measurements and errors over time and the time course for each source amplitude is handled as a weighted sum of basis functions.

The connectivity or functional connectome is such a problem since it deals with time lags of 1-100's of msec. For this problem the measurements are the virtual recordings extracted from MEG measurements at specific locations, i.e. the consensus views [2.G]. These are assumed to be due to (1) axial currents in nearby axon bundles due to passage of volleys of actions potentials and (2) population post synaptic currents in nearby gray matter due to the arrival of volleys of action potentials. We plan to use High Definition Fiber Tractography [14] to identify fiber tracts and neural populations likely coupled to them. The virtual recordings from sources found near these structures will be used as the measurements to determine the coupling strength of the neural populations to the fiber tract and the propagation times/velocities of the action potential volleys

All variables, parameters, and matrices in the formalism presented here are over the real numbers only. The key properties of these mathematical objects on which the formalism relies are (1) the existence of an inverse for any non-zero number and any non-singular matrix and (2) distributivity of multiplication over addition. These properties hold for the complex numbers, the quaternions, and the octonions, hence referee consensus optimization will likely work over these number systems. Thorough analysis of this assertion remains[20].

References

[1] Sarvas J. 1987. Basic mathematical and electromagnetic concepts of the biomagnetic inverse problem. Phys Med Biol 32(1): 11-22.

[2] Hämäläinen MS, Ilmoniemi R., 1984. Interpreting

[18] The threshold for significance for a single voxel was $\chi^2 \geq 28.4$, $p \leq 3 \times 10^{-7}$. In the worst case for multiple comparisons, i.e. $2mm^3$ voxels, the chance that a single voxel out of 200,000 will reach the selected significance threshold is 0.06. The minimum number of voxels reaching the threshold is ≈400. The chance for that worst case is $p < 0.06^{400}$.

[19] In the more general formulation, more than 1 amplitude variable may be used for each source. 2 or 3 are used in the MEG problem.

[20] The formal argument in appendix 1.B relies on associativity which is not a property of quaternions.

measured magnetic fields of the brain: Estimates of current distributions. Techical Report TKK-F-A559.

[3] Pascual-Marqui RD; Michel CM; Lehmann D. October 1994. Low-Resolution electromagnetic tomography – A new method for localizing electrical activity in the brain. Intl J Psychophys 18(1):49-65.

[4] Pascual-Marqui RD. 2002. Standardized low resolution brain electromagnetic tomography (sLORETA): technical details. Methods & Findings in Experimental & Clinical Pharmacology 2002, 24D:5-12. URL last visited Dec 2010: Open Access HTML

[5] Huang MX, Dale AM, Song T, Halgren E, Harrington DL, Podgorny I, Canive JM, Lewis S, Lee RR. 2006. Vector-based spatial–temporal minimum L1-norm solution for MEG NeuroImage 31 1025 – 1037.

[6] Huang MX, Theilmann RJ, Robb A, Angeles A, Nichols S, Drake A, D'Andrea J, Levy M, Holland M, Song T, Ge S, Hwang E, Yoo K, Cui L, Baker DG, Trauner D, Coimbra R, Lee RR. August 2009. Integrated Imaging Approach with MEG and DTI to Detect Mild Traumatic Brain Injury in Military and Civilian Patients J Neurotrauma 26:1213–1226.

[7] Krieger D, S Onodipe, PJ Charles, RJ Sclabassi. Real time signal processing in the clinical setting. Annals of Biomedical Engineering Vol 26: 462-472, 1998.

[8] Anderson E, Bai Z, Bischof C, Blackford S, Demmel J, Dongarra J, Du Croz J, Greenbaum A, Hammarling S, McKenney A, Sorensen D. 22 Aug 1999. LAPACK Users' Guide Release 3.0. Open Access HTML (Last visited Dec2010).

[9] Krieger D, McNeil M, Zhang J, Schneider W, Li X, Okonkwo DO. Referee consensus: A platform technology for nonlinear optimization. XSEDE13 Proceedings of the Conference on Extreme Science and Engineering Discovery Environment: Gateway to Discovery, San Diego, 2013. Open Access PDF

[10] Zhang J, G Sudre, X Li, W Wang, D Weber, A Bagic. Task-related MEG source localization via discriminant analysis. Proceedings 33rd Intl. Conf. IEEE EMBS: 2351-2354, 2011.

[11] Douglas Cheyne, Leyla Bakhtazad, and William Gaetz 2006. Spatiotemporal Mapping of Cortical Activity Accompanying Voluntary Movements Using an Event-Related Beamforming Approach. Human Brain Mapping 27:213–229.

[12] Robinson SE, Vrba J 1999. Functional neuroimaging by synthetic aperture magnetometry. In: Yoshimine T, Kotani M, Kuriki S, Karibe H, Nakasato N, editors. Recent Advances in Biomagnetism: Proceedings From the 11th International Conference on Biomagnetism. Sendai: Tokoku University Press. p 302–305.

[13] He B, Coleman T, Genin GM, Glover G, Hu X, Johnson N, Liu T, Makeig S, Sajda P, Ye K. Grand Challenges in Mapping the Human Brain: NSF Workshop Report. IEEE Trans Biomed Engr, Vol 60, No. 11 , November, 2013: 2983-2992. Open Access PDF

[14] Verstynen T, Jarbo K, Pathak S, Schneider W. 2011 In vivo mapping of microstructural somatotopies in the human corticospinal pathways. J Neurophys 105(1): 336-346.

APPENDICES

A. Zeroes of the inverse solution for the instantaneous referee consensus system. Suppose we have measures, $\vec{B} = \langle b_1 \ \cdots \ b_j \ \cdots \ b_J \rangle$, which contain a contribution from source $\mathbf{d_k}$, i.e.: $\vec{B}^{\mathbf{T}} = \begin{matrix} b_1 = \mathbf{h_{1,k}}\mathbf{d_k} + \delta_1 \\ \vdots \\ b_j = \mathbf{h_{j,k}}\mathbf{d_k} + \delta_j \\ \vdots \\ b_J = \mathbf{h_{J,k}}\mathbf{d_k} + \delta_J \end{matrix}$. The δ's are due to the contributions of all other source, known and unknown. We use the inverse solution for the contributions of this group of sources which includes $\mathbf{d_k}$, $\vec{D} = \langle d_1 \ \cdots \ \mathbf{d_k} \ \cdots \ d_K \rangle$: $\vec{D}^{\mathbf{T}} = \left(\left(\mathbf{H}^{\mathbf{T}}\mathbf{H} \right)^{-1} \mathbf{H}^{\mathbf{T}} \right) \vec{B}^{\mathbf{T}} = \mathbf{\Xi}\vec{B}^{\mathbf{T}}$ by substituting in the inverse solution from the J equations for the measurements, $\vec{B}^{\mathbf{T}}$:

$$\begin{pmatrix} d_1 \\ \vdots \\ d_k \\ \vdots \\ d_K \end{pmatrix} = \mathbf{\Xi} \begin{pmatrix} \mathbf{h_{1,k}}\mathbf{d_k} + \delta_1 \\ \vdots \\ \mathbf{h_{j,k}}\mathbf{d_k} + \delta_j \\ \vdots \\ \mathbf{h_{J,k}}\mathbf{d_k} + \delta_J \end{pmatrix} = \mathbf{\Xi} \begin{pmatrix} \mathbf{h_{1,k}}\mathbf{d_k} \\ \vdots \\ \mathbf{h_{j,k}}\mathbf{d_k} \\ \vdots \\ \mathbf{h_{J,k}}\mathbf{d_k} \end{pmatrix} + \mathbf{\Xi} \begin{pmatrix} \delta_1 \\ \vdots \\ \delta_j \\ \vdots \\ \delta_J \end{pmatrix}.$$

Since $\begin{pmatrix} \mathbf{h_{1,k}}\mathbf{d_k} \\ \vdots \\ \mathbf{h_{j,k}}\mathbf{d_k} \\ \vdots \\ \mathbf{h_{J,k}}\mathbf{d_k} \end{pmatrix}$ is the k^{th} column of $\mathbf{H}$ and $\mathbf{\Xi H} = \left(\left(\mathbf{H}^{\mathbf{T}}\mathbf{H} \right)^{-1} \mathbf{H}^{\mathbf{T}} \right) \mathbf{H} = \mathbf{I}$, the identity,

$$\mathbf{\Xi} \begin{pmatrix} \mathbf{h_{1,k}}\mathbf{d_k} \\ \vdots \\ \mathbf{h_{j,k}}\mathbf{d_k} \\ \vdots \\ \mathbf{h_{J,k}}\mathbf{d_k} \end{pmatrix} = \begin{pmatrix} 0 \\ \vdots \\ \mathbf{d_k} \\ \vdots \\ 0 \end{pmatrix}, \text{ therefore } \begin{pmatrix} d_1 \\ \vdots \\ \mathbf{d_k} \\ \vdots \\ d_K \end{pmatrix} = \begin{pmatrix} 0 \\ \vdots \\ \mathbf{d_k} \\ \vdots \\ 0 \end{pmatrix} + \mathbf{\Xi} \begin{pmatrix} \delta_1 \\ \vdots \\ \delta_j \\ \vdots \\ \delta_J \end{pmatrix}.$$

In other words, the only source for which the inverse solution includes a contribution from the measurements due to $\mathbf{d_k}$ is $\mathbf{d_k}$. All others have a contribution from the measurements due to $\mathbf{d_k}$ of 0 ..

B. Referee selection. There are 2 related conditions which must hold regarding referee selection.

- The causal matrix, $\mathbf{H}$, must have full column rank to insure that the inverse solution, $\vec{D}^{\mathbf{T}} = \left(\left(\mathbf{H}^{\mathbf{T}}\mathbf{H} \right)^{-1} \mathbf{H}^{\mathbf{T}} \right) \vec{B}^{\mathbf{T}} = \mathbf{\Xi}\vec{B}^{\mathbf{T}}$, will exist.
- Each referee must be "correlated" with the test location. In particular as before, if $\begin{pmatrix} \mathbf{h_{1,k}} \\ \vdots \\ \mathbf{h_{j,k}} \\ \vdots \\ \mathbf{h_{J,k}} \end{pmatrix} = \vec{\mathbf{h}}_{\mathbf{k}}^{\mathbf{T}}$ is the column

of $\mathbf{H}$ corresponding to the test location and $\begin{pmatrix} h_{1,\kappa\neq k} \\ \vdots \\ h_{j,\kappa\neq k} \\ \vdots \\ h_{J,\kappa\neq k} \end{pmatrix} = \vec{h}^{\mathbf{T}}_{\kappa\neq k}$ is a column of $\mathbf{H}$ corresponding to a referee, then $\vec{h}^{\mathbf{T}}_{\kappa\neq k} \bullet \vec{\mathbf{h}}^{\mathbf{T}}_{\mathbf{k}} \neq 0$.

The two conditions are somewhat at odds since condition 1 requires that the columns of $\mathbf{H}$ are independent while condition 2 requires that they not be orthogonal. The need for this non-orthogonality condition can be seen as follows. Suppose the opposite, that $\vec{h}^{\mathbf{T}}_{\kappa\neq k} \bullet \vec{\mathbf{h}}^{\mathbf{T}}_{\mathbf{k}} = 0$. And suppose we have measurements with a contribution from the test location, i.e.

$$\begin{aligned} b_1 &= \mathbf{h}_{\mathbf{J,k}}\mathbf{d}_{\mathbf{k}} + \delta_1 \\ &\vdots \\ b_j &= \mathbf{h}_{\mathbf{j,k}}\mathbf{d}_{\mathbf{k}} + \delta_j \\ &\vdots \\ b_J &= \mathbf{h}_{\mathbf{J,k}}\mathbf{d}_{\mathbf{k}} + \delta_J \end{aligned}$$

. And suppose further that we exclude the test location from $\hat{\mathbf{H}}$.We apply the inverse solution to these measurements:

$$\begin{pmatrix} d_1 \\ \vdots \\ d_{\kappa\neq k} \\ \vdots \\ d_K \end{pmatrix} = \Xi \begin{pmatrix} \mathbf{h}_{1,\mathbf{k}}\mathbf{d}_{\mathbf{k}} + \delta_1 \\ \vdots \\ \mathbf{h}_{\mathbf{j,k}}\mathbf{d}_{\mathbf{k}} + \delta_j \\ \vdots \\ \mathbf{h}_{\mathbf{J,k}}\mathbf{d}_{\mathbf{k}} + \delta_J \end{pmatrix} = \Xi \begin{pmatrix} \mathbf{h}_{1,\mathbf{k}}\mathbf{d}_{\mathbf{k}} \\ \vdots \\ \mathbf{h}_{\mathbf{j,k}}\mathbf{d}_{\mathbf{k}} \\ \vdots \\ \mathbf{h}_{\mathbf{J,k}}\mathbf{d}_{\mathbf{k}} \end{pmatrix} + \Xi \begin{pmatrix} \delta_1 \\ \vdots \\ \delta_j \\ \vdots \\ \delta_J \end{pmatrix}$$

. The first of these terms, $\Xi \begin{pmatrix} \mathbf{h}_{1,\mathbf{k}}\mathbf{d}_{\mathbf{k}} + \delta_1 \\ \vdots \\ \mathbf{h}_{\mathbf{j,k}}\mathbf{d}_{\mathbf{k}} + \delta_j \\ \vdots \\ \mathbf{h}_{\mathbf{J,k}}\mathbf{d}_{\mathbf{k}} + \delta_J \end{pmatrix}$, is the bleed through at each of the K sources from the contribution of the source at the test location. We isolate and expand this term:

$$\Xi \begin{pmatrix} \mathbf{h}_{1,\mathbf{k}}\mathbf{d}_{\mathbf{k}} \\ \vdots \\ \mathbf{h}_{\mathbf{j,k}}\mathbf{d}_{\mathbf{k}} \\ \vdots \\ \mathbf{h}_{\mathbf{J,k}}\mathbf{d}_{\mathbf{k}} \end{pmatrix} = \left(\left(\hat{\mathbf{H}}^{\mathbf{T}}\hat{\mathbf{H}} \right)^{-1} \hat{\mathbf{H}}^{\mathbf{T}} \right) \begin{pmatrix} \mathbf{h}_{1,\mathbf{k}}\mathbf{d}_{\mathbf{k}} \\ \vdots \\ \mathbf{h}_{\mathbf{j,k}}\mathbf{d}_{\mathbf{k}} \\ \vdots \\ \mathbf{h}_{\mathbf{J,k}}\mathbf{d}_{\mathbf{k}} \end{pmatrix} = \left(\left(\hat{\mathbf{H}}^{\mathbf{T}}\hat{\mathbf{H}} \right)^{-1} \right) \left(\hat{\mathbf{H}}^{\mathbf{T}} \begin{pmatrix} \mathbf{h}_{1,\mathbf{k}}\mathbf{d}_{\mathbf{k}} \\ \vdots \\ \mathbf{h}_{\mathbf{j,k}}\mathbf{d}_{\mathbf{k}} \\ \vdots \\ \mathbf{h}_{\mathbf{J,k}}\mathbf{d}_{\mathbf{k}} \end{pmatrix} \right).$$

But for $\left(\hat{\mathbf{H}}^{\mathbf{T}} \begin{pmatrix} \mathbf{h}_{1,\mathbf{k}}\mathbf{d}_{\mathbf{k}} \\ \vdots \\ \mathbf{h}_{\mathbf{j,k}}\mathbf{d}_{\mathbf{k}} \\ \vdots \\ \mathbf{h}_{\mathbf{J,k}}\mathbf{d}_{\mathbf{k}} \end{pmatrix} \right)$, the κ^{th} entry is zero since the κ^{th} row of $\hat{\mathbf{H}}^{\mathbf{T}}$ is $\vec{h}^{\mathbf{T}}_{\kappa\neq k}$, the κ^{th} column of $\hat{\mathbf{H}}$, and $\vec{h}^{\mathbf{T}}_{\kappa\neq k} \bullet \vec{\mathbf{h}}^{\mathbf{T}}_{\mathbf{k}} = 0$. In other words, there is no bleed through to the κ^{th} referee from the test location. Hence this referee location is not usable for generating a referee template.

Don Krieger Dr. Krieger has research interests in clinical neurophysiology, MEG, signal processing, real time high throughput data processing, and fusion of anatomic and functional brain imaging.

Malcolm McNeil Dr. McNeil's research interests include neurogenic speech and language disorders, information processing and comprehension, differential diagnosis of aphasia and traumatic brain injury, and test design and development, and fusion of anatomic and functional brain imaging.

Jinyin Zhang Dr. Zhang has research interests in MEG and functional brain imaging.

Ava Puccio Dr. Puccio has research interests in improvement of outcome in traumatic brain injury, controlled normothermia, mechanisms of brain oxygenation, and genetic variances and expression on outcome.

Walter Schneider Dr. Schneider has research interests in attention, learning, cognitive neuroscience, and fusion of anatomic and functional brain imaging.

Xin Li Dr. Li has research interests in integrated circuits and biomedical signal processing.

David O. Okonkwo Dr. Okonkwo has research interests in traumatic brain and spinal injury, spinal deformity, MEG, and fusion of anatomic and functional brain imaging.